Molecular Modeling of the Adsorption of an Egg Yolk Protein on a Water–Oil Interface

Molecular Modeling of the Adsorption of an Egg Yolk Protein on a Water-Oil Interface

Alessio Lombardo Pontillo, Marco Ferrari, Marcello Rospiccio, and Antonio Buffo*

Department of Applied Science and Technology, Politecnico di Torino, Corso Duca degli Abruzzi 24, 10129, Torino, Italy

E-mail: antonio.buffo@polito.it

Abstract

Egg yolk contains several molecular species with emulsifying properties, such as proteins and phospholipids. In particular, these molecules have both polar and non-polar parts and thus can act as surfactants. One of the most surface-active proteins from egg yolk low-density lipoproteins is the so-called Apovitellenin-1. Experimental studies have been hindered by the difficulties in isolating individual species from egg yolk lipoproteins. The purpose of this work was to assess the emulsifying properties of Apovitellenin-1 and any potential cooperative or competitive behavior in the presence of phospholipids. To do so, molecular simulations were carried out in a liquid-liquid interfacial system, consisting of water and soybean oil, with varying concentrations of phospholipids and for different spatial configurations. To evaluate the conformational stability of the protein at the water-oil interface, the Gibbs free energy was computed from Metadynamics simulations as a function of the distance from the interface and of the radius of gyration. Moreover, a detailed analysis was also performed to determine which peptide residues were responsible for the protein adsorption at the oil-water interface, as well as the lowering of the interfacial tension. Lastly, we combined the sim-

ulation results with a thermodynamic model to predict the interfacial tension behavior at increasing protein bulk concentration, which cannot be measured experimentally.

Keywords

Protein, Interface, Molecular Dynamics, Metadynamics, Surfactants

Introduction

Emulsions are frequently used in the food industry and one of the most renowned examples is surely mayonnaise. Emulsions are obtained starting from two or more immiscible fluids, typically an aqueous and an oil phase. In the case of mayonnaise, small oil droplets are dispersed into a continuous water phase by vigorous agitation,[1] for example in a rotor-stator mixer.[2,3] Usually, food emulsions, which are included in the class of macroemulsions, are thermodynamically unstable as they are characterized by a dimension of the oil droplets ranging from 0.2 to 50 μm.[4,5] Due to this instability, after the emulsion has been formed, oil droplets begin to approach each other until they coalesce to form larger droplets. When a drop is large enough, it separates from the aqueous phase and emerges at the surface, thus this process can eventually lead to complete phase separation.[6] The speed of this process can be influenced by several physical-chemical factors, such as the type of the two fluids, the droplet size, the presence of molecules able to prevent phase separation, and the mixing method.[1] Instead, nanoemulsions and microemulsions have droplet sizes ranging from 10 to 100 nm. However, the former are thermodynamically unstable as macroemulsions, while the latter are isotropic and thermodynamically stable systems.[7]

Mayonnaise is formed by mixing egg yolk, oil, water, salt, vinegar and lemon juice. The two immiscible phases are oil and water, with the latter being one of the ingredients as well as being contained in the egg yolk. Vinegar and lemon juice, which give flavor to the mayonnaise, reduce the pH, thus improving the stability of emulsions.[8] Egg yolk is

the key ingredient as it contains biomolecules that can act as surfactants at the water-oil interface, namely phospholipids and proteins.[1,9] Surfactant molecules consist of both polar and non-polar parts, which can interact with the water and the oil phase, respectively, by positioning themselves at the interface, thus limiting droplet coalescence and preventing phase separation.[10]

Among the proteins found in the egg yolk, the so-called Apovitellenin-1[11,12] is the one with the highest surface activity and with the greatest emulsifying potential. It is a homodimer made up of two identical polypeptide chains of 82 residues each (approx 9 kDa), with a disulfide bond between the cysteine residues in position 75 of each chain.[11–13] There is limited information regarding this protein as it is unstable in water and, thus, difficult to isolate.[12,14] Furthermore, its spatial structure has not been determined experimentally. Apovitellenin-1 is found in the low-density lipoproteins (LDLs) of egg yolk, along with other proteins, phospholipids, triglycerides, and cholesterol. When the LDLs reach the water-oil interface, they break and release the surfactant molecules. Therefore, proteins and phospholipids are free to diffuse at the interface, leading to a decrease in the interfacial tension, thus stabilizing the emulsion.[15,16]

Molecular Dynamics (MD) and Metadynamics (MetaD) simulations have been largely employed in order to investigate protein interactions at interfaces.[17–26] Thus, the objective of this work is to study the behavior of the Apovitellenin-1 at the water-oil interface with and without phospholipids, using both MD and MetaD techniques. Specifically, MetaD is based on MD but has the advantage of performing a probabilistic sampling of rare and transitional events,[27] such as those involving protein dynamics at interfaces. These approaches are commonly adopted to study phenomena that may not be directly observed in experimental works.[28] Although experimental techniques capable of addressing particle adsorption at liquid-liquid interfaces exist,[29,30] some of which with remarkable details,[31–33] the above mentioned computational approaches were deemed to be more advantageous for this study, especially considering the difficulty in isolating Apovitellenin-1 from egg yolk.

In this perspective, this work introduces a novel approach, utilizing atomistic models and statistical analyses, to gain a mechanistic understanding of the adsorption behavior of an egg yolk protein at the oil-water interface, as well as its interactions with other co-surfactants. Furthermore, to relate the interfacial tension decrease associated with protein adsorption to the protein bulk concentration, a thermodynamic model of protein adsorption was developed and applied to the case investigated. This model was obtained by combining our results with those of previous works[34,35], in which another molecular approach, namely Dissipative Particle Dynamics (DPD), was employed. In such a way, it was shown how molecular techniques could potentially be used to predict equilibrium properties that are otherwise difficult to measure experimentally.

Materials and Methods

The theoretical basis of the two main molecular techniques employed in this work (MD and MetaD) is explained in the Supporting Information, giving more emphasis on the Well-Tempered Metadynamics (WTMetaD) which is the specific method adopted here. Hence, the next sections present the computational details, the thermodynamic model of protein adsorption, and the model validation employed.

Molecular Simulations

Molecular Modeling

In this section, some details about the chemical species involved in this work, namely the protein (Apovitellenin-1), the oil phase, water, and the phospholipids, are presented, together with all the necessary hypotheses and approximations. First, it is important to underline that the sequence of the mature protein is available at the UniProtKB database[36] (`www.uniprot.org/uniprot/P02659`), under the accession number P02659. For further analyses, two applications were used: AlphaFold[37,38] and H++.[39] AlphaFold predicts different spatial

structures for the protein, starting from its amino acid sequence. Each structure is associated with an index of prediction, called lDDT (Local Distance Difference Test), a superposition-free score that evaluates local distance differences of all atoms in a model, which varies between 0 and 100, indicating the accuracy of the prediction.[40] For this work, the structure with the highest value of the index of prediction was used, as shown in the Supporting Information. Moreover, it can be noticed that the region encompassing the disulfide bond was correctly represented and was predicted with the highest index of the molecule. The second application, H++, was used to predict the protonation state of each amino acid residue. By providing the structure and the pH value of interest (here considered equal to 3.8), H++ returns the pKa for each amino acid in the protein. If the pH is less than the pKa then the functional group of the residue will be protonated, otherwise it will be deprotonated. This leads to a total charge for the protein equal to $+14e^{-}$.

For the oil phase, it was also necessary to adopt some simplifications. In particular, the non-aqueous phase consists of soybean oil, whose fatty acid composition is reported in Table 1.[41] It was thus assumed that all the triglycerides contain only one type of fatty acid,

Table 1: Fatty acids composition of soybean oil.[41]

Fatty acid	**Fatty acid content, wt%**	
	Range	**Average**
Palmitic (PM)	7-12	10.7
Stearic (ST)	2-5.5	3.9
Oleic (OL)	20-50	22.8
Linoleic (LL)	35-60	50.8
Linolenic (LN)	2-13	6.8

that is without an internal distribution. In this way, the composition reported in Table 1 is considered as the weight fraction of triglycerides in the soybean oil. Hence, the number of molecules that compose the oil phase in the simulation box reflects such composition. All the information about structural conformation and topology for the triglycerides was obtained by using LigParGen.[42–44]

The TIP3P model was used for water. This model is characterized by a low computational

cost, but it can not simulate the correct behavior of water at temperatures near 0 °C.[45,46] A 50/50 volume ratio was assumed for the oil and water phases.

To model phospholipids, only 1-palmitoyl-2-oleoyl-sn-glycero-3-phosphocholine (POPC) was taken into account since it was identified as the most abundant in the egg yolk.[9,47,48] The structural information regarding the phospholipids was obtained from the Slipids website.[48,49]

Simulation Setup

MD simulations were performed using GROMACS 2020.6.[50] All the systems were simulated using the Verlet list for neighboring atoms with a cut-off of 1.0 nm for both Coulomb and van der Waals interactions and the Particle Mesh Ewald summation (PME)[51] for electrostatic calculations. Periodic Boundary Conditions (PBC) were considered in all three directions. Since the protein has a non-zero net-total charge, an appropriate number of Cl^- ions was added to the system to achieve electrostatic neutrality. For all systems energy minimization was first carried out with a steepest descent minimization that was stopped when the maximum force between atoms was lower than 1000 kJ/mol/nm, followed by two equilibration steps: 100 ps in NVT (Isothermal–Isovolumetric ensemble) and 1 ns in NPT (Isothermal-Isobaric ensemble), using the Berendsen thermostat,[52] with pressure coupling for NPT simulations. The pressure was set equal to 1 bar and temperature was fixed at 298 K. Production runs were instead performed with the Parrinello-Rahman barostat[53] (relaxation time equal to 2 ps) and the V-rescale thermostat[54] (relaxation time equal to 0.1 ps). MD production was carried out with a time step equal to $\Delta t = 2$ fs for a total number of steps $N_G = 5 \times 10^7$. The OPLS-AA force field[55] was employed to compute the interactions between all the atoms in the system. Hydrogen bonds were constrained with the LINCS algorithm[56] and TIP3P[45,46,57] water molecules were kept rigid with the SETTLE algorithm.[58] Four cases were analyzed in this study, as reported in Table 2 with the corresponding box

Table 2: System compositions in terms of the number of molecules for the cases investigated in this work, together with box sizes.

Case	Protein	Water	Oil[i]					POPC	Cl^-	Box Dimensions [nm³]
			PM	ST	OL	LL	LN			X × Y × Z
1	1	55845	132	42	263	602	88	0	14	12.15 × 24.30 × 12.15
2	1	55065	132	42	263	602	88	10[ii]	14	12.15 × 24.30 × 12.15
3	1	42619	90	30	172	452	61	216[iii]	14	11.70 × 23.40 × 11.70
4	1	42619	90	30	172	452	61	432[iv]	14	11.70 × 23.40 × 11.70

[i] See Table 1 for references on triglyceride molecule types.
[ii] Free in the water bulk, concentration equal to that found in egg yolk.
[iii] Placed at the oil-water interface, concentration equal to half of the saturation.
[iv] Placed at the oil-water interface, concentration equal to saturation.

dimensions.

To create the first system from Table 2, the oil phase was initially set up. Starting from a box with dimensions $X = Y = Z = 25.00$ nm, the five types of triglyceride molecules were randomly inserted in a number corresponding to the proportions of Table 1. After the energy minimization and the equilibration steps, the box reached the dimensions $X = Y = Z =$ 12.15 nm. Then, the box was extended in the Y-dimension and a single protein molecule was placed in the center of the void phase. In this way, we can assume that the protein does not interact with both interfaces at the same time, since the minimum distance between the protein and each interface is larger than the cut-off used for non-bonded interactions. The remaining space was then solvated with water, thus creating the interface between oil and water. After that, fourteen molecules of water were replaced with an equal number of Cl^- ions. This system was used as the basis for the other three cases. For the second case, a sufficient number of water molecules were replaced with ten molecules of POPC. Such number was calculated from the number of POPC molecules per protein molecule ratio ($N_{\mathrm{POPC}}/N_{\mathrm{P}}$), knowing the mass of each molecular species[11,12] ($m_{\mathrm{P}} = 18677.38$ Da is the protein mass and $m_{\mathrm{POPC}} = 760.09$ Da is the POPC mass) and their corresponding mass fraction in the egg yolk,[9,47] as shown in Table 3 and Eq. 1.

Table 3: Fraction of proteins and phospholipids in the egg yolk.[9,47]

Fraction of LDL in the dried egg yolk (χ_{LDL})	0.66
Fraction of protein in LDL (χ_{P})	0.10
Fraction of lipids in the dried egg yolk (χ_{L})	0.63
Fraction of phospholipids in lipids (χ_{PL})	0.33
Fraction of phosphatidylcholines in phospholipids (χ_{PC})	0.76
Fraction of POPC in phosphatidylcholine (χ_{POPC})	0.154

$$\frac{N_{\mathrm{POPC}}}{N_{\mathrm{P}}} = \frac{\chi_{\mathrm{L}} \times \chi_{\mathrm{PL}} \times \chi_{\mathrm{PC}} \times \chi_{\mathrm{POPC}}}{\chi_{\mathrm{LDL}} \times \chi_{\mathrm{P}}} \times \frac{m_{\mathrm{P}}}{m_{\mathrm{POPC}}} = 9.05 \approx 10 \ . \tag{1}$$

The value of $N_{\mathrm{POPC}}/N_{\mathrm{P}}$ was rounded up to compensate for possible approximation errors. In fact, the exact concentration of Apovitellenin-1 in the egg yolk is not known,[11,12,14] so it was assumed that all LDL proteins were molecules of Apovitellenin-1. For the remaining two systems (Cases 3 and 4 of Table 2), the box from Case 1 was used as a starting point, although with a smaller volume. This difference was due to the fact that after substituting some of the water and the oil molecules with the POPC molecules, a part of the box remained void. It was thus necessary to perform another equilibration in an NPT ensemble where the volume of the box was reduced to fill the void space with other molecules.

The saturation concentration of POPC phospholipids at the water-oil interface is 0.635 nm^2/lipid.[48] Thus, by knowing the superficial area of the interface, it was possible to calculate the number of phospholipid molecules to insert into the simulation box, in order to achieve a concentration equal to half that of the saturation (Case 3) and equal to the saturation one (Case 4). It is important to stress that there are two interfaces in each system due to the periodic boundary conditions. Hence, the phospholipids were placed at each interface by removing an equal volume of water and oil. The phospholipids were already positioned in the correct orientation, with the polar part towards the water phase and the non-polar part near the oil phase. In summary, Figure 1 shows the snapshots of the four cases studied here.

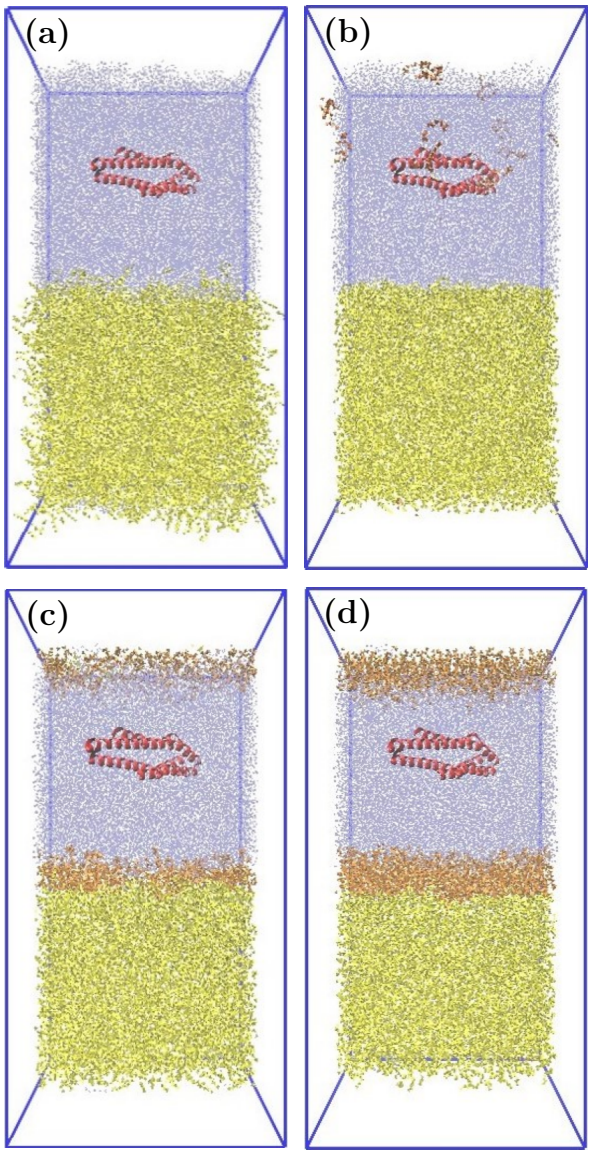

Figure 1: Snapshots realized with the VMD software[59] of the simulated systems corresponding to the four cases from Table 2 (Case 1 (a), Case 2 (b), Case 3 (c), Case 4 (d)), where the protein, POPC, water, and oil molecules are represented in red, orange, blue, and yellow, respectively. To have a clearer view, some solvent molecules were hidden.

Well-Tempered Metadynamics Simulations

The PLUMED v.2.7.2[60,61] plugin was used to perform all Well-Tempered Metadynamics simulations. The collective variables chosen for all MetaD simulations were the protein radius of gyration, used as a metric for denaturation, and the distance between the protein center of mass and the oil phase. To reduce the computational cost, a further simplification was adopted: for each molecule of the oil phase, only a single atom of carbon was considered, which was found only among the molecules of the oil phase. Specifically, the number density along the y direction (i.e. orthogonal to the interface) was compared for all the atoms of the oil phase and for the chosen carbon atom, to ensure the accuracy of this approximation. More details are reported in the corresponding section of the Supporting Information. The bias factor was equal to 10, while the initial Gaussian height was set to 1 kJ/mol and the Gaussian deposition rate to 1 hill/ps. Lastly, the free energy surfaces (FES) and the probability distributions of the CVs were obtained by using the reweighting approach proposed by Tiwary and Parrinello[62]. To verify the convergence of the biased simulations, the variation of the CVs over the last 10% of the simulation time was computed. These results are reported in the Supporting Information as well.

Thermodynamic Model of Protein Adsorption

The adsorption mechanism of proteins at fluid interfaces is significantly different from that of common surfactants, such as non-ionic single-chained amphiphilic molecules with a hydrophilic head and a hydrophobic tail.[63] In particular, a common feature of all surfactant proteins is the typical S-shaped trend of the surface pressure at increasing protein surface concentration.[63] Among other things, the thermodynamic model of protein adsorption was successfully employed to evaluate the protein adsorption energy at fluid interfaces from experimental data.[64] In this work instead the adsorption energy of the Apovitellenin-1 at the oil/water interface was obtained from metadynamics simulations. This information was then transferred to the thermodynamic model, in which the parameter calibration was based on

previous results obtained by means of DPD simulations.[34] It is eventually possible to predict a macroscopic behavior of the protein investigated, namely the surface pressure curve at increasing protein bulk concentration.

The theory of protein adsorption, which is described in detail in the work of Fainerman et al.[63], is based on the idea that the protein molecule can exist in multiple states in the interfacial layer. The large exposed surface area and the large number of possible conformations of an adsorbed protein molecule can be modeled as a significant increase in the non-ideality of the surface entropy. This is the reason why the most simple isotherm models (e.g. Henry, Langmuir, Frumkin) cannot describe protein adsorption[63]. In contrast, the thermodynamic model of protein adsorption proposed by Fainerman et al.[63] assumes that the partial molar area of the protein molecules can vary between a maximum (ω_{max}), at very low surface coverage, and a minimum (ω_{min}) value, at high surface coverage. The molar areas of two adjacent conformations differ from each other by the value ω_0, which corresponds to the molar area of the solvent and is assumed to be significantly smaller than that of the protein in any state. Furthermore, the total number of possible states of the protein molecule, n, is defined by the above-mentioned parameters, so that $\omega_0 = \Delta\omega = (\omega_{max} - \omega_{min})/(n-1)$. Thus, the following equation of state was derived:

$$-\frac{\pi\omega_0}{RT} = \ln(1-\omega\Gamma) + \Gamma(\omega-\omega_0) + a(\omega\Gamma)^2 \ , \tag{2}$$

where $\pi = \sigma_0 - \sigma$ is the surface pressure, σ_0 and σ are the interfacial tensions of the free interface and of that covered by protein surfactants, respectively, R is the ideal gas constant, T the temperature and a is a Frumkin-type intermolecular interaction parameter. $\Gamma = \sum_{i=1}^{n} \Gamma_i$ is the total adsorption of protein in all n states, $\theta = \omega\Gamma = \sum_{i=1}^{n} \omega_i\Gamma_i$ is the total surface coverage, and ω is the average molecular area of adsorbed proteins. The equation of

the adsorption isotherm for each state (j) of the protein is given by:

$$b_j c = \frac{\omega\Gamma_j}{(1-\omega\Gamma)^{\frac{\omega_j}{\omega}}} \exp\left(-2a\left(\frac{\omega_j}{\omega}\right)\omega\Gamma\right) , \tag{3}$$

where c is the protein bulk concentration and b_j is the adsorption equilibrium constant for the protein in the j-state. Moreover, it can be assumed that all constants b_j have one and the same value for all states j from $i = 1$ to $i = n$, and therefore the adsorption constant for the protein molecule is given by $b = \sum_j b_j = nb_j$. This assumption allows to define each of the individual Γ_i in terms of the total adsorption, thus providing the distribution function of adsorptions over various states of the protein molecule:

$$\Gamma_j = \Gamma \frac{(1-\omega\Gamma)^{\frac{\omega_j-\omega_{min}}{\omega}} \exp\left(2a\Gamma(\omega_j-\omega_{min})\right)}{\sum_{i=1}^{n}(1-\omega\Gamma)^{\frac{\omega_i-\omega_{min}}{\omega}} \exp\left(2a\Gamma(\omega_i-\omega_{min})\right)} , \tag{4}$$

while the average molecular area of adsorbed proteins ω can be expressed as follows:

$$\omega = \frac{\sum_{i=1}^{n}\omega_i(1-\omega\Gamma)^{\frac{\omega_i-\omega_{min}}{\omega}} \exp\left(2a\Gamma(\omega_i-\omega_{min})\right)}{\sum_{i=1}^{n}(1-\omega\Gamma)^{\frac{\omega_i-\omega_{min}}{\omega}} \exp\left(2a\Gamma(\omega_i-\omega_{min})\right)} . \tag{5}$$

The thermodynamic model presented above describes the adsorption behavior at low protein concentrations very satisfactorily, where the simultaneous increase of surface pressure and adsorption is observed.[63,65] However, assuming the existence of a critical protein concentration, denoted c^*, π^* and Γ^*, above which the surface pressure remains almost constant as the adsorption often increases, the model can be extended to account for higher concentrated solutions.[63] Thus, for $c > c^*$ the equation of state and the adsorption isotherm respectively become:

$$-\frac{\pi\omega_0}{RT} = \frac{1}{\Psi}[\ln(1-\omega\Gamma) + \Gamma(\omega-\omega_0) + a(\omega\Gamma)^2] , \tag{6}$$

and

$$b_j c = \frac{\omega\Gamma_j}{(1-\omega\Gamma)^{\frac{\omega_j}{\omega\Psi}}} \exp\left(-2a\left(\frac{\omega_j}{\Psi\omega}\right)\omega\Gamma\right) , \tag{7}$$

respectively, with:

$$\Psi = \frac{\Gamma}{\Gamma^*} \exp\left(\varepsilon \frac{\pi - \pi^*}{RT} \omega\right), \tag{8}$$

where ε represents an adjustable parameter. Lastly, the adsorption equilibrium constant b can be expressed as:[64]

$$b = \frac{1}{\rho} \exp\left(-\frac{\Delta G_{ads}}{RT}\right), \tag{9}$$

where ρ is the molar concentration of the solvent, assumed to be equal to 56 mol/l for dilute aqueous solutions.[66] It is important to highlight that the value of ΔG_{ads} was here computed from MetaD simulations, thus representing the link between the molecular modeling technique and the macroscopic thermodynamic theory.

The equations of state Eqs. 2 and 6 were solved together with the expression of the mean molar area Eq. 5, to find the value of ω for each Γ value. Then, these values were included in the isotherm of adsorption (Eqs. 3 and 7) in order to obtain the surface pressure profile as a function of the protein bulk concentration. To do this, further parameter optimization was performed with Matlab R2022b, to minimize the error between the fitting curve for Eqs. 2 and 6 and the data from dissipative particle dynamics simulations.[34] The optimized parameters used in the thermodynamic model have been listed in Table 4.

Table 4: Optimized parameters used in the thermodynamic model of protein adsorption (from Eqs. 2 to 8).

Parameter	**Optimized value**
a	0.00625
ω_{min} [m^2/mol]	1.9×10^{6}
ω_{max} [m^2/mol]	4.9×10^{7}
n	565
ε	3.9×10^{-4}
π^* [mN/m]	22.5

Model Validation

In addition to the cases already described, another simulation study was conducted to validate the approach used in this work. As mentioned before, to the best of the Authors' knowledge, there is no experimental data available in the literature regarding the isolated Apovitellenin-1 to be compared with the results obtained from our simulations. Therefore, the same methodology was tested for a similar application, whose details are available. In particular, the system described in the work of Maldonado-Valderrama et al.[67] was reproduced and modeled with the same simulation parameters used for the case of Apovitellenin-1. Therefore, for the sake of the comparison, the system consists of β-casein adsorbing at the air-water interface. The air phase was treated as a vacuum.[17] The structure of β-casein was obtained from UniProt (code P02666, `www.uniprot.org/uniprot/P02666`).[36] After adjusting the protonation state of the peptide residues with H++ at a pH of 7.4, the protein was placed at the center of the water bulk. The box construction was made analogously to the previous case of Apovitellenin-1. Then, box charge neutralization, energy minimization, and equilibration (1 ns in NVT ensemble) were conducted. The OPLS-AA force field was used again here. To maintain the water-air interface, it was necessary to perform the simulation in the NVT ensemble, by fixing the temperature equal to 298 K with the V-rescale thermostat. Regarding the MetaD setup, the same parameters of the simulation of Apovitellenin-1 were used. Indeed, the two collective variables were the protein's radius of gyration and the distance of the protein center of mass from the water-air interface. Since, in this case, the simulation was conducted in the NVT ensemble, the energy obtained from MetaD is the Helmholtz free energy. One can switch to the Gibbs free energy ΔG_{ads} by applying the following expression:[68]

$$\Delta G_{ads} = \Delta F_{MetaD} = \left[-\frac{1}{\beta} \int_{y_a}^{y_b} e^{-\beta F_y(y)} dy \right] - \left[-\frac{1}{\beta} \int_{y_c}^{y_d} e^{-\beta F_y(y)} dy \right] \tag{10}$$

where β is the inverse of the temperature and Boltzmann constant product, $F_y(y)$ is the Helmholtz free energy obtained from MetaD simulations along the y direction, and (y_a, y_b) and (y_c, y_d) are the adsorption and bulk region, respectively, which are arbitrarily chosen.

Results and Discussion

Figure 2 shows illustrative snapshot examples of the protein adsorbed at the oil/water interface for cases 1 (a) and 4 (b). As it can be seen, the presence of a phospholipid layer at the oil/water interface prevented full adsorption of the protein, which will be discussed in detail later on. The free energy surfaces (FES) obtained from MetaD simulations give an overview

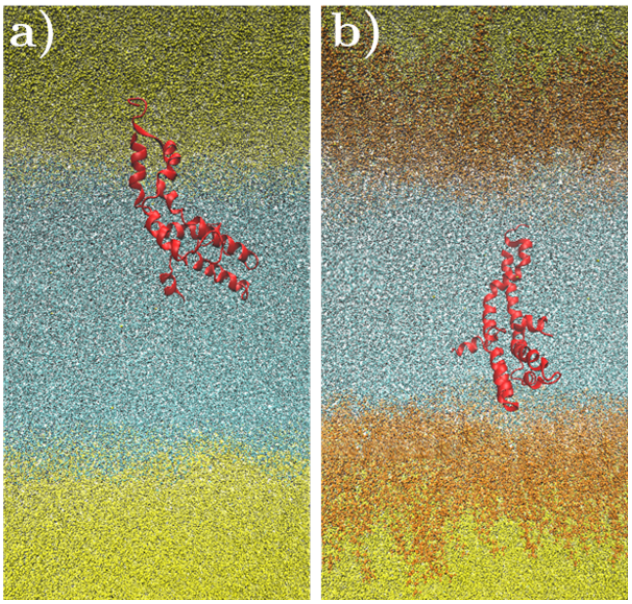

Figure 2: Illustrative snapshot examples of the simulated systems realized with the VMD software:[59] a) Case 1, protein adsorbed at the oil/water interface; b) Case 4, protein adsorption in the presence of the phospholipid layer at the oil/water interface. Protein, POPC, water, and oil molecules are represented in red, orange, blue, and yellow, respectively.

of the collective variable space explored by each of the four cases. They are represented in the Supporting Information by varying both the two collective variables. It should be noted that energy is considered here the Gibbs free energy, as these simulations were conducted in the NPT ensemble. However, in order to have a clearer representation, the probabilities

associated with the various states were also calculated and reported in Figure 3, where the peaks correspond to the most probable configurations of the system. As shown in Figure 3(a), the protein was fully adsorbed on the water-oil interface only in cases 1 and 2. It is important to underline that the minimum distance was calculated considering the protein center of mass and not the closest atom to the oil-water interface, thus the highest peak of probability was slightly shifted towards values slightly greater than 0. Instead, in cases 3 and 4, the highest probability peaks were shifted to larger distances from the oil-water interface due to the steric hindrance caused by the presence of phospholipids at the interface. Therefore, the protein positioned itself near the oil-water interface without being able to be completely adsorbed. In fact, it may be noted that the distance between the protein and the interface in case 4 was larger than in case 3. This is due to the fact that in case 4 there was a higher concentration of phospholipids at the interface, which hindered the adsorption of the protein even more than in case 3. Accordingly, in case 4 there was a higher probability of finding the protein in the water bulk compared to case 3, as indicated by the second-highest peak. However, it may be observed from Figure 3(a) that case 1 and case 2 had approximately the same trend for distances smaller than 3 nm, thus suggesting that the phospholipids in solution were not able to prevent protein adsorption. Nevertheless, the presence of phospholipids in case 2 made the probability profiles smoother (Figure 3), thus the peak in the water bulk at a distance from the interface equal to 5.5 nm was not present, as instead observed for case 1. This is shown in detail in Figure 4, where the protein energy profiles of cases 1 and 2 are represented as a function of the distance from the interface. From these profiles, the protein Gibbs free energy of adsorption ΔG_{ads} at the oil-water interface can be estimated as the difference in the values of the energy associated with the protein at a distance close and far from the interface as reported in Figure 4. Therefore, the presence of free phospholipids affected the absolute value of ΔG_{ads}. In fact, for case 1 ΔG_{ads} amounted to -108.18 kJ/mol, while ΔG_{ads} was equal to -122.71 kJ/mol for case 2, meaning that, when free phospholipids are initially present in water bulk, this made the protein adsorption even

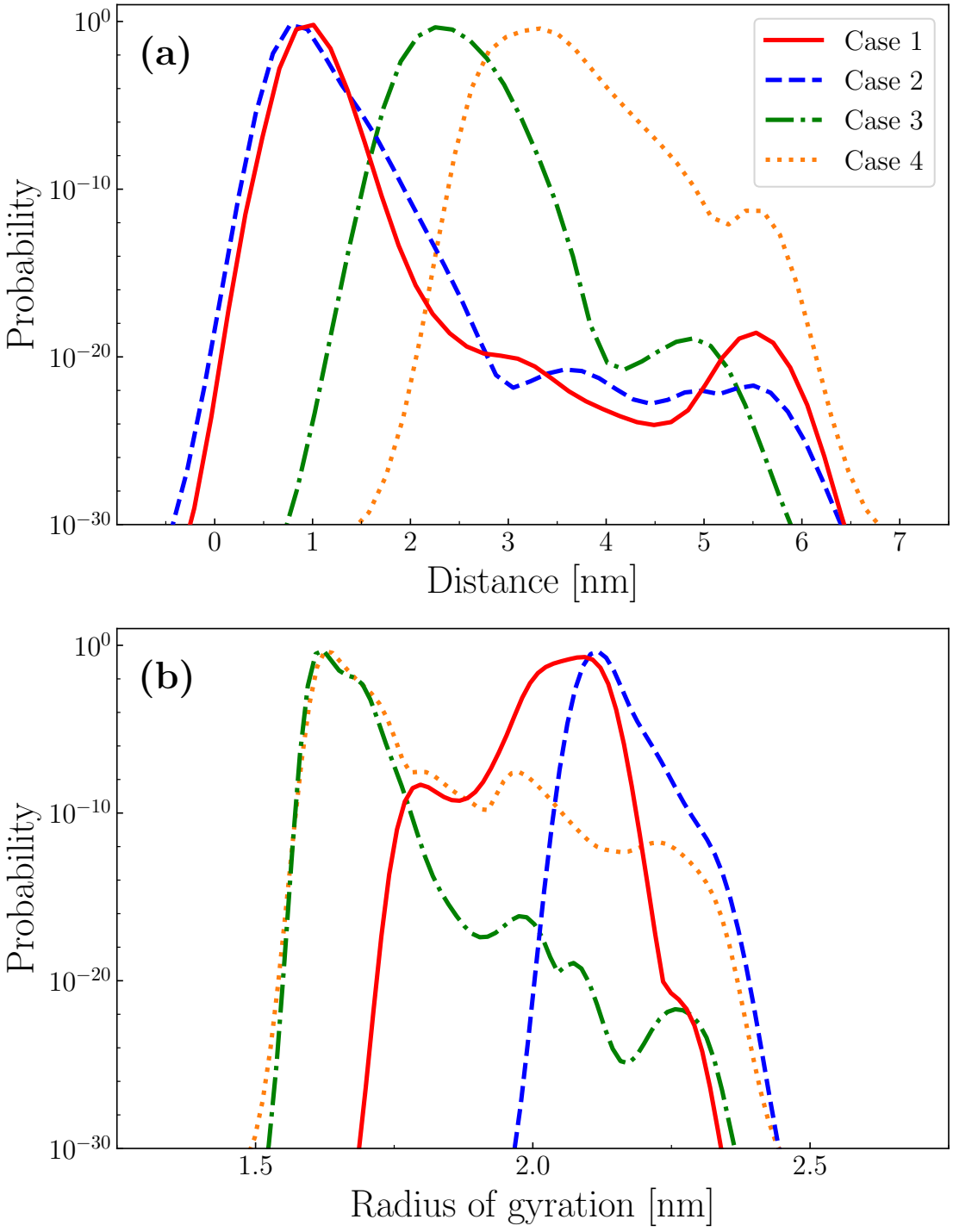

Figure 3: Probability (logarithmic) distributions of the distance of Apovitellenin-1 from the oil-water interface (a) and of the protein radius of gyration (b). Case 1: no phospholipids (red continuous line); Case 2: phospholipids in the water bulk (blue dashed line); Case 3: phospholipids at the water-oil interface at a concentration equal to half of the saturation (green dash-dot line); Case 4: phospholipids at the water-oil interface at a concentration equal to saturation (orange dotted line).

more likely to occur in case 2 rather than in case 1. Moreover, these values of ΔG_{ads} are consistent with those reported in the literature for protein surfactants.[69] The presence of phospholipids in the water bulk had an effect also on the radius of gyration, as shown in Figure 3(b) (red continuous line and blue dashed line). Despite the fact that in both cases 1 and 2 the maximum probability peak corresponded to a value of the radius of gyration equal to 2.125 nm, when the phospholipids were not present (Case 1) the protein explored a wider range of values and, specifically, more compact structures. This was also true for Cases 3 and 4 where, although the phospholipids were present at even higher concentrations, their accumulation at the interface resulted in fewer interactions with the protein, thus promoting compact structures and limiting protein adsorption. This is most likely related to the fact that the protein molecule becomes smaller when trying to penetrate the phospholipid layer. In Case 4 (Figure 3(b), orange dotted line) with a saturated phospholipids interface, the protein can explore approximately the same region of the radius of gyration value as in Case 3 (Figure 3(b), green dash-dotted line) but with a higher probability of occurrence. However, in Case 2, the distribution of the radius of gyration was clearly shifted towards higher values, thus looser structures, suggesting a denaturing effect exerted by free phospholipids in solution.

To provide a better understanding of the relative interactions between protein and phospholipids, Figure 5 shows the density profiles along the direction normal to the oil-water interface and the radial distribution functions of the protein with respect to phospholipids for cases 2, 3, and 4. As can be seen, when phospholipids were initially free in the water bulk (case 2), they were then adsorbed at the oil-water interface together with the protein. A stronger interaction of the non-polar tails rather than of the polar heads can indicate a protein denaturation effect (Figure 5(d)) due to the high non-polar component in the protein structure. This can also justify a wider protein radius of gyration explored in case 2 compared to case 1 when phospholipids are not present (Figure 3(b)). Moreover, the denaturation effect may be responsible for the flatter protein energy profile of Figure 4(b) in

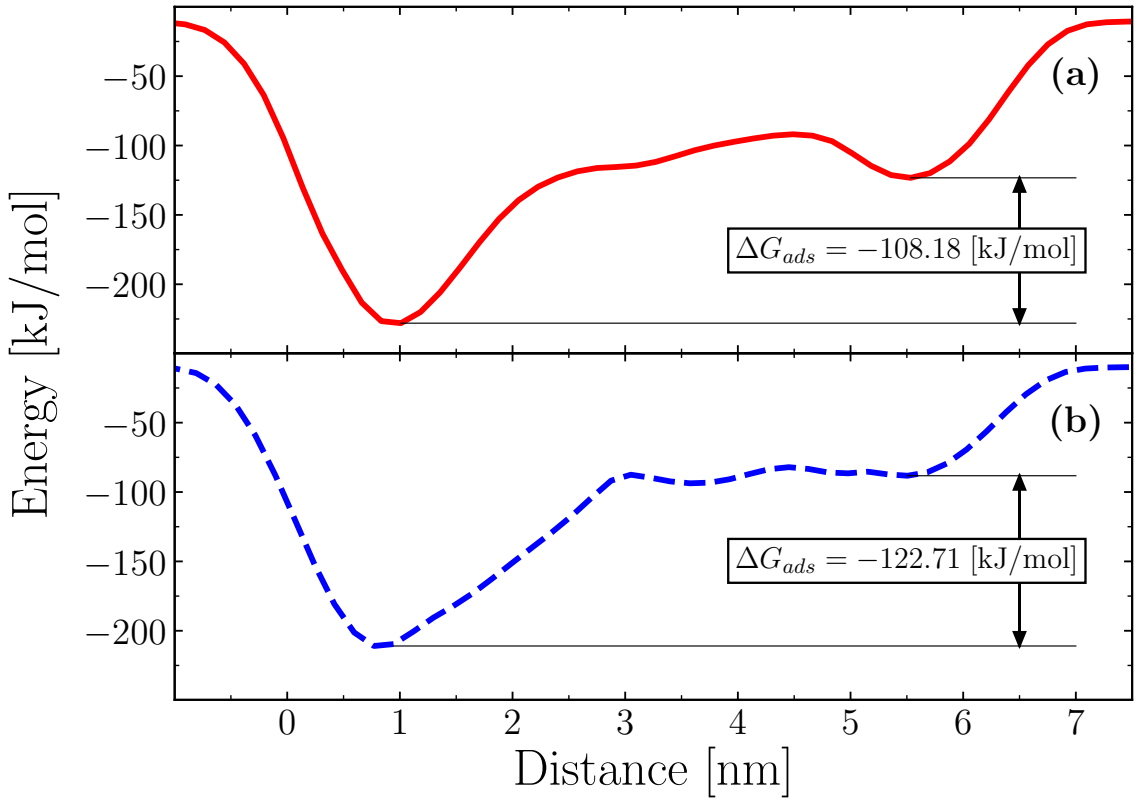

Figure 4: Protein energy profiles and determination of the Gibbs free energy of adsorption at the oil-water interface. (a) Case 1: no phospholipids; (b) Case 2: phospholipids in the water bulk at a concentration calculated from Eq. 1.

water bulk and higher free Gibbs energy of adsorption (in absolute value) with respect to case 1. Therefore, the strong interaction of non-polar tails can explain how the presence of free phospholipids promotes protein adsorption at the oil-water interface. On the other hand, when phospholipids were initially adsorbed at the interface (cases 3 and 4), the relative interaction between the protein and phospholipids polar heads shown in Figures 5(e) and (f) may be the reason of the steric hindrance making the protein not fully adsorbed at the interface and of a more compact structure with respect to cases 1 and 2 (Figure 3(b)). It is also important to note that the higher the concentration of adsorbed phospholipids the larger the distance of the protein from the interface as reported in Figures 5(b) and (c), shifting the peaks in the radial distribution functions of Figures 5(e) and (f).

For case 1, a more detailed analysis was conducted to investigate which peptide residues were involved in the adsorption process. Figure 6 shows the probability of finding each amino acid residue as a function of the distance from the interface. As can be seen, the region of the protein involved in the adsorption the most is strongly hydrophobic, hence they tend to adsorb onto the non-polar oil interface. To provide better visualization, points with a probability higher than 0.9 were highlighted by red dots. It is worth mentioning that, apart from the portion of the protein adsorbed (the red dots in Figure 6), the remaining part of the amino acid residues were free to move in the region close to the interface. For this reason, the other probability values are lower than 0.3.

Application of the Thermodynamic Model of Protein Adsorption

Simulation results of case 1 were then used to build the thermodynamic model of protein adsorption. Once the optimized parameter set was obtained (Table 4), it was verified that the equation of state of the thermodynamic model of protein adsorption (Eqs. 2 and 6) fitted the data obtained from DPD simulations[34] with an acceptable error, as shown in Figure 7(a). Although different water/fluid interfaces were considered, a very good agreement was also noticed between the values of Apovitellenin-1 at the oil-water interface and those obtained

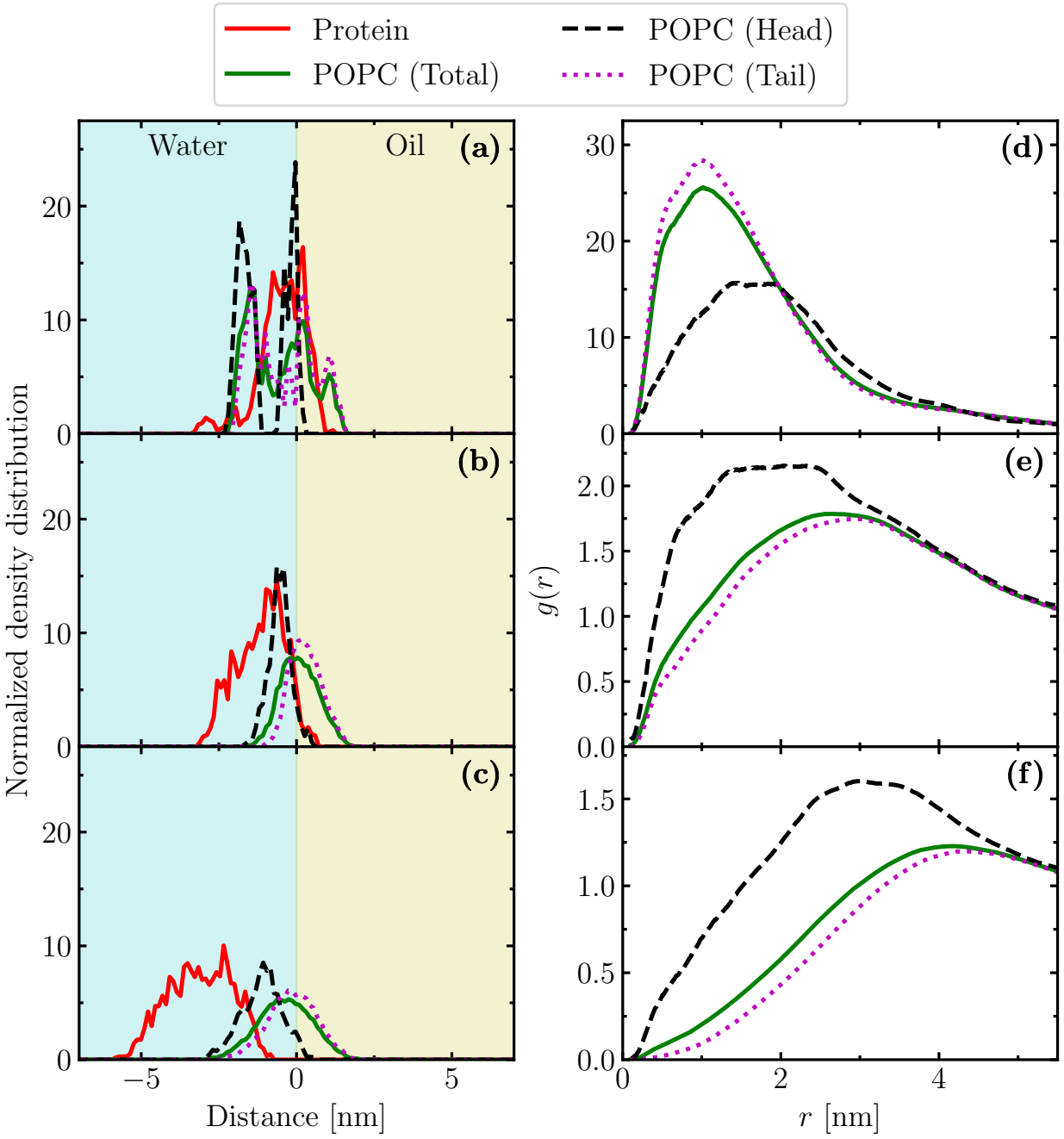

Figure 5: Density profiles along the direction normal to the oil-water interface ((a), (b), and (c)) and radial distribution functions of the protein molecule with respect to phospholipids ((d), (e), and (f)) for cases 2 ((a) and (d)), 3 ((b) and (e)), and 4 ((c) and (f)). To highlight the differences in the curves of the right plots, the vertical axis scale is accordingly defined.

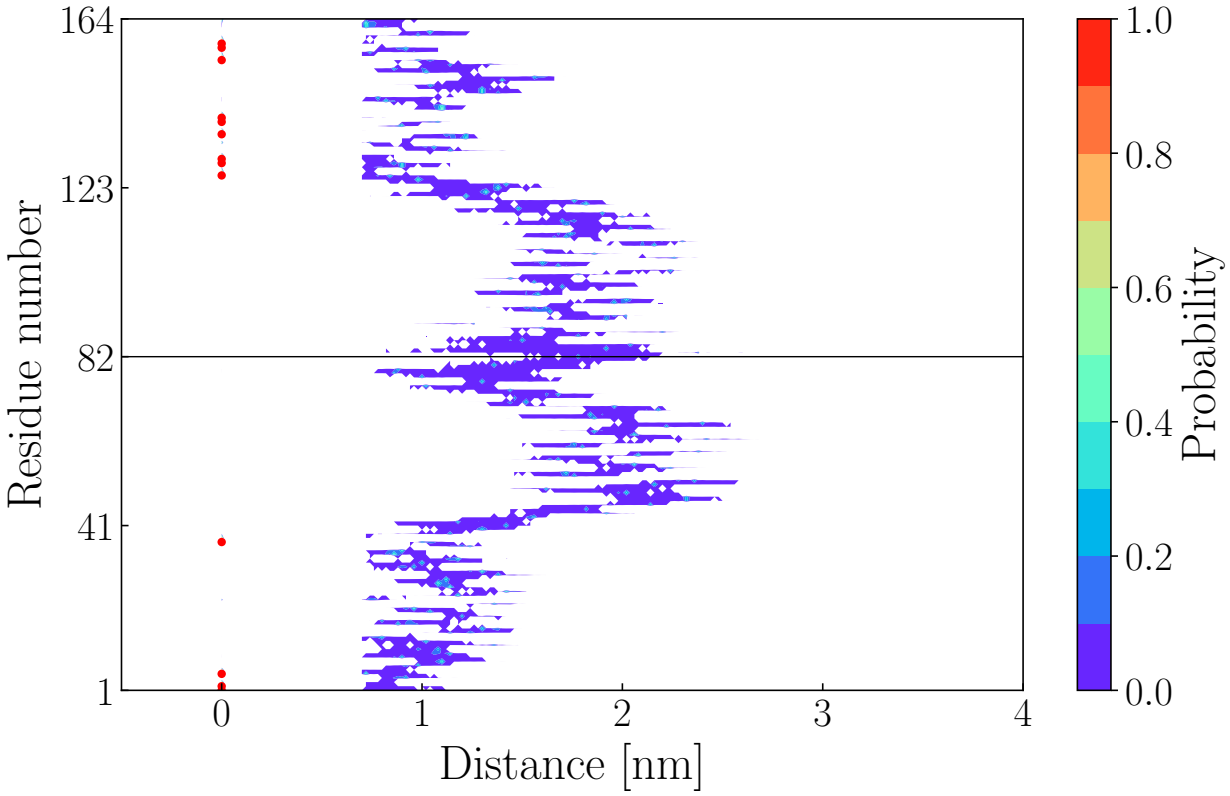

Figure 6: Probability contour plot as a function of the distance from the oil-water interface for each amino acid residue. The red dots highlight the amino acid residues mostly involved in the protein adsorption with a probability higher than 0.9. The black line shows the division between the two chains of Apovitellenin-1.

experimentally for the β-casein at the air-water interface.[65] This result would suggest that these two proteins may have very similar behavior, typical of flexible protein surfactants compared to globular ones at liquid/fluid interfaces.[63,64] Therefore, this consideration would support the choice of using the data of β-casein to validate our approach, as reported later. To obtain a complete thermodynamic description of adsorption for the Apovitellenin-1, only the adsorption equilibrium constant b is required and can be obtained by means of Eq. 9. As reported, b only depends on the value of ΔG_{ads}. Therefore, from the MetaD simulation of case 1, the variation of the Gibbs free energy between the protein in the bulk state and the protein in the adsorbed state was obtained (Figure 4). Once the constant of adsorption was obtained, it was included in the expression of the adsorption isotherm (Eqs. 3 and 7) to find the value of the protein bulk concentration for each value of π and Γ obtained from DPD simulations,[34] as reported in Figure 7. Although the bulk concentration values appeared to be relatively small compared to those of β-casein,[65] to the best of the authors' knowledge there are no experimental data of Apovitellenin-1 to directly compare this result. Nevertheless, this trend represents a prediction of a macroscopic property that is difficult to experimentally measure for the protein under investigation.

Since this profile only depends on the value of b and, in turn, on the Gibbs free energy of adsorption ΔG_{ads}, the approach and results proposed here were eventually validated by investigating the adsorption at the air-water interface of β-casein, whose value of ΔG_{ads} is available in the literature.[64,67] In this last case, the experiment with the β-casein from the work of Maldonado-Valderrama et al.[67] was reproduced by MD and MetaD approaches with the same setup adopted for the Apovitellenin-1 simulations. The most important result here was the value of the Gibbs free energy of adsorption $\Delta G_{\beta-cas,MetaD} = -52.11$ kJ/mol, calculated by applying Eq. 10 to the Helmholtz free energy profile reported in the Supporting Information. This value is very similar to the one found in the literature which is $\Delta G_{\beta-cas,Exp} = -59.4$ kJ/mol.[64,67] It is thus reasonable to consider the trend of Figure 7(b) a valid result.

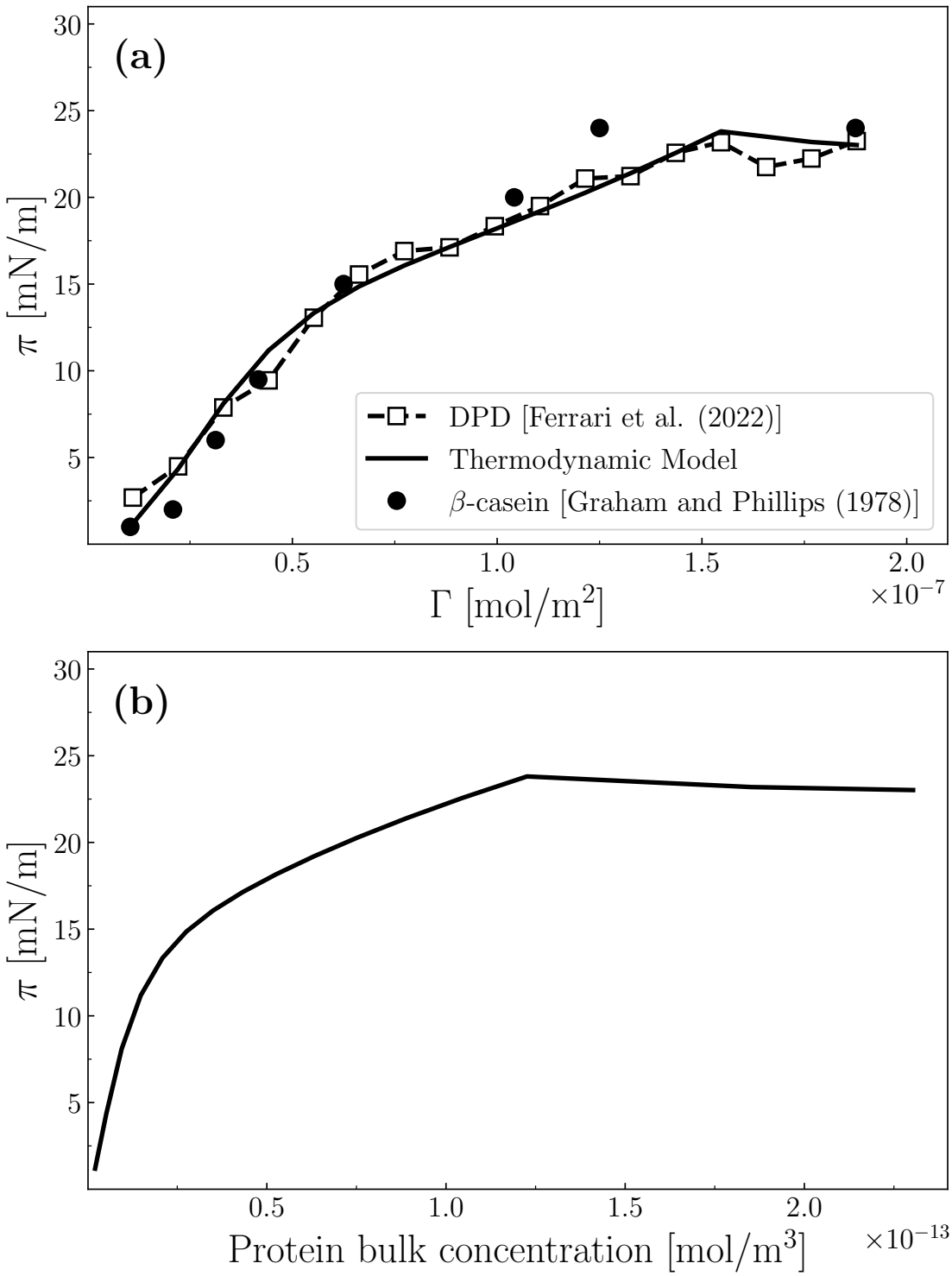

Figure 7: Variation of the surface pressure versus the protein surface molar concentration (a) and versus the protein bulk concentration (b). The squares represent the data obtained from DPD simulations for the Apovitellenin-1.[34,70] The continuous line represents the thermodynamic model of protein adsorption applied to the Apovitellenin-1. The circles represent the experimental data of β-casein at the air-water interface.[65]

Conclusions

Apovitellenin-1, one of the proteins responsible for the stability of food emulsions like mayonnaise, is not stable in aqueous solvents and it is difficult to separate from the other species of the egg yolk. Therefore, an attempt to study its adsorption behavior at a water-oil interface, at different phospholipids concentrations, using molecular dynamics and metadynamics was made. At low concentrations, phospholipids promoted protein adsorption by further reducing the structural stability of the protein in water. Instead, at higher phospholipids concentrations, namely starting from concentrations equal to half of the saturation, they could sterically inhibit the adsorption of the protein. Furthermore, when phospholipids were free in solution, they shifted the distribution of radius of gyration towards higher values, suggesting a loosening action on the protein structure. Conversely, when the phospholipids accumulated at the interface, despite their concentration being higher, they promoted more compact structures. Lastly, the hydrophobic peptide residues were found to be responsible for protein adsorption at the interface. Subsequently, a thermodynamic model of protein adsorption was also built in order to evaluate the trend of the surface pressure at increasing protein surface and bulk concentration. In particular, the equation of state for the Apovitellenin-1 presented a very similar trend to that of another protein surfactant, namely β-casein. The Gibbs free energy of protein adsorption at the oil-water interface was extracted from metadynamics simulations and it was linked to previous Dissipative Particle Dynamics simulations,[34] to obtain a complete description of the Apovitellenin-1 as a surfactant. This result shows how molecular modeling techniques could be used not only to reproduce qualitative behaviors but also to quantitatively predict properties that are difficult to estimate experimentally. To support this claim, the value of the Gibbs free energy for the β-casein was also predicted from metadynamics simulations, and was found to be very similar to the one obtained experimentally.[64,67] In future works, it would also be interesting to explore the critical surface concentration of phospholipids at which the protein is able to adsorb at the interface. This may represent an important application of the method here proposed, since

the greatest synergistic effect between phospholipids and proteins in decreasing the surface tension could be studied and, as a consequence, a better understanding of the stability of food emulsions would be achieved.

Acknowledgement

We acknowledge the CINECA award under the ISCRA initiative, for the availability of high-performance computing resources. Computational resources were also provided by HPC@POLITO, a project of Academic Computing within the Department of Control and Computer Engineering at the Politecnico di Torino (`http://www.hpc.polito.it`). We also thank Professor Francesca Bosco from the Department of Applied Science and Technology at Politecnico di Torino for her help in interpreting the results. Finally, we thank Andrea Arsiccio, Ph.D., and Professor Daniele Marchisio for their valuable suggestions to carry out this work.

Supporting Information Available

The Supporting Information is available free of charge. A brief description of the theoretical background, additional computational details, and further analyses.

References

(1) Harrison, L. J.; Cunningham, F. E. Factors influencing the quality of mayonnaise: a review. *J. Food Qual.* **1985**, *8*, 1–20.

(2) Dubbelboer, A.; Janssen, J. J. M.; Hoogland, H.; Zondervan, E.; Meuldijk, J. Pilot-scale production process for high internal phase emulsions: Experimentation and modeling. *Chem. Eng. Sci.* **2016**, *148*, 32–43.

(3) Ferrari, M.; Boccardo, G.; Buffo, A.; Vanni, M.; Marchisio, D. L. CFD simulation of a high-shear mixer for food emulsion production. *J. Food Eng.* **2023**, *358*, 111655.

(4) Das, K.; Kinsella, J. In *Stability Of Food Emulsions: Physicochemical Role Of Protein And Nonprotein Emulsifiers*; Kinsella, J. E., Ed.; Advances in Food and Nutrition Research; Academic Press, 1990; Vol. 34; pp 81–201.

(5) McClements, D. J. Critical Review of Techniques and Methodologies for Characterization of Emulsion Stability. *Crit. Rev. Food Sci. Nutr.* **2007**, *47*, 611–649.

(6) Mackson, J. P.; Singh, S. P. The effect of temperature and vibration on emulsion stability of mayonnaise in two different package types. *Packag. Technol. Sci.* **1991**, *4*, 81–90.

(7) McClements, D. J. Nanoemulsions versus microemulsions: terminology, differences, and similarities. *Soft Matter* **2012**, *8*, 1719–1729.

(8) Depree, J. A.; Savage, G. P. Physical and flavour stability of mayonnaise. *Trends Food Sci. Technol.* **2001**, *12*, 157–163.

(9) Anton, M. In *Bioactive Egg Compounds*; Huopalahti, R., López-Fandiño, R., Anton, M., Schade, R., Eds.; Springer Berlin Heidelberg: Berlin, Heidelberg, 2007; pp 1–6.

(10) Urbina-Villalba, G. Effect of Dynamic Surfactant Adsorption on Emulsion Stability. *Langmuir* **2004**, *20*, 3872–3881.

(11) Anton, M.; Martinet, V.; Dalgalarrondo, M.; Beaumal, V.; David-Briand, E.; Rabesona, H. Chemical and structural characterisation of low density lipoproteins purified from hen egg yolk. *Food Chem.* **2003**, *83*, 175–183.

(12) Jolivet, P.; Boulard, C.; Beaumal, V.; Chardot, T.; Anton, M. Protein Components of Low-Density Lipoproteins Purified from Hen Egg Yolk. *J. Agric. Food Chem.* **2006**, *54*, 4424–4429.

(13) Zambrowicz, A.; Pokora, M.; Setner, B.; Dąbrowska, A.; Szołtysik, M.; Babij, K.; Szewczuk, Z.; Trziszka, T.; Lubec, G.; Chrzanowska, J. Multifunctional peptides derived from an egg yolk protein hydrolysate: Isolation and characterization. *Amino acids* **2014**, *47*, 369–380.

(14) Burley, R. W. Studies on the Apoproteins of the Major Lipoprotein of the Yolk of Hen's Eggs III. Influence of Salt Concentration During Isolation on the Amount and Composition of the Apoproteins. *Aust. J. Biol. Sci.* **1978**, *31*, 587–592.

(15) Anton, M. Egg yolk: structures, functionalities and processes. *J. Sci. Food Agric.* **2013**, *93*, 2871–2880.

(16) Yang, Y.; Jin, H.; Jin, Y.; Jin, G.; Sheng, L. A new insight into the influence of pH on the adsorption at oil-water interface and emulsion stability of egg yolk protein. *Int. J. Biol. Macromol.* **2023**, *246*, 125711.

(17) Rospiccio, M.; Arsiccio, A.; Winter, G.; Pisano, R. The Role of Cyclodextrins against Interface-Induced Denaturation in Pharmaceutical Formulations: A Molecular Dynamics Approach. *Mol. Pharmaceutics* **2021**, *18*, 2322–2333.

(18) Zare, D.; Allison, J. R.; McGrath, K. M. Molecular Dynamics Simulation of β-Lactoglobulin at Different Oil/Water Interfaces. *Biomacromolecules* **2016**, *17*, 1572–1581.

(19) Zare, D.; McGrath, K. M.; Allison, J. R. Deciphering β-Lactoglobulin Interactions at an Oil–Water Interface: A Molecular Dynamics Study. *Biomacromolecules* **2015**, *16*, 1855–1861.

(20) Hagiwara, T.; Sakiyama, T.; Watanabe, H. Molecular Simulation of Bovine β-Lactoglobulin Adsorbed onto a Positively Charged Solid Surface. *Langmuir* **2009**, *25*, 226–234.

(21) Wei, T.; Carignano, M. A.; Szleifer, I. Lysozyme Adsorption on Polyethylene Surfaces: Why Are Long Simulations Needed? *Langmuir* **2011**, *27*, 12074–12081.

(22) Liu, J.; Liao, C.; Zhou, J. Multiscale Simulations of Protein G B1 Adsorbed on Charged Self-Assembled Monolayers. *Langmuir* **2013**, *29*, 11366–11374.

(23) Peng, C.; Liu, J.; Zhao, D.; Zhou, J. Adsorption of Hydrophobin on Different Self-Assembled Monolayers: The Role of the Hydrophobic Dipole and the Electric Dipole. *Langmuir* **2014**, *30*, 11401–11411.

(24) Cheung, D. L. Molecular Simulation of Hydrophobin Adsorption at an Oil–Water Interface. *Langmuir* **2012**, *28*, 8730–8736.

(25) Euston, S. R. Molecular Dynamics Simulation of Protein Adsorption at Fluid Interfaces: A Comparison of All-Atom and Coarse-Grained Models. *Biomacromolecules* **2010**, *11*, 2781–2787.

(26) Tang, Y.; Liu, Y.; Zhang, D.; Zheng, J. Perspectives on Theoretical Models and Molecular Simulations of Polymer Brushes. *Langmuir* **2024**, *40*, 1487–1502.

(27) Laio, A.; Parrinello, M. Escaping Free-Energy Minima. *Proc. Natl. Acad. Sci. U. S. A.* **2002**, *99*, 12562–12566.

(28) Frenkel, D.; Smit, B. In *Understanding Molecular Simulation (Second Edition)*, second edition ed.; Frenkel, D., Smit, B., Eds.; Academic Press: San Diego, USA, 2002; pp 1–6.

(29) Hitaishi, P.; Seth, A.; Mitra, S.; Ghosh, S. K. Thermodynamics and In-Plane Viscoelasticity of Anionic Phospholipid Membranes Modulated by an Ionic Liquid. *Pharm. Res.* **2022**, *39*, 2447–2458.

(30) Ravera, F.; Loglio, G.; Kovalchuk, V. I. Interfacial dilational rheology by oscillating bubble/drop methods. *Curr. Opin. Colloid Interface Sci.* **2010**, *15*, 217–228.

(31) Smits, J.; Giri, R. P.; Shen, C.; Mendonça, D.; Murphy, B.; Huber, P.; Rezwan, K.; Maas, M. Synergistic and Competitive Adsorption of Hydrophilic Nanoparticles and Oil-Soluble Surfactants at the Oil-Water Interface. *Langmuir* **2021**, *37*, 5659–5672.

(32) Smits, J.; Prasad Giri, R.; Shen, C.; Mendonça, D.; Murphy, B.; Huber, P.; Rezwan, K.; Maas, M. Assessment of nanoparticle immersion depth at liquid interfaces from chemically equivalent macroscopic surfaces. *J. Colloid Interface Sci.* **2022**, *611*, 670–683.

(33) Mandal, P.; Giri, R. P.; Murphy, B. M.; Ghosh, S. K. Self-Assembly of Graphene Oxide Nanoflakes in a Lipid Monolayer at the Air-Water Interface. *ACS Appl. Mater. Interfaces* **2021**, *13*, 57023–57035.

(34) Ferrari, M.; Handgraaf, J.-W.; Boccardo, G.; Buffo, A.; Vanni, M.; Marchisio, D. L. Molecular modeling of the interface of an egg yolk protein-based emulsion. *Phys. Fluids* **2022**, *34*, 021903.

(35) Ferrari, M.; Boccardo, G.; Marchisio, D. L.; Buffo, A. Application of dissipative particle dynamics to interfacial systems: Parameterization and scaling. *AIP Adv.* **2023**, *13*, 035324.

(36) The UniProt Consortium, UniProt: the universal protein knowledgebase in 2021. *Nucleic Acids Res.* **2020**, *49*, D480–D489.

(37) Jumper, J.; Evans, R.; Pritzel, A.; Green, T.; Figurnov, M.; Ronneberger, O.; Tunyasuvunakool, K.; Bates, R.; Žídek, A.; Potapenko, A.; Bridgland, A.; Meyer, C.; Kohl, S. A. A.; Ballard, A. J.; Cowie, A.; Romera-Paredes, B.; Nikolov, S.; Jain, R.; Adler, J.; Back, T.; Petersen, S.; Reiman, D.; Clancy, E.; Zielinski, M.; Steinegger, M.; Pacholska, M.; Berghammer, T.; Bodenstein, S.; Silver, D.; Vinyals, O.; Senior, A. W.; Kavukcuoglu, K.; Kohli, P.; Hassabis, D. Highly accurate protein structure prediction with AlphaFold. *Nature* **2021**, *596*, 583–589.

(38) Mirdita, M.; Schütze, K.; Moriwaki, Y.; Heo, L.; Ovchinnikov, S.; Steinegger, M. ColabFold: making protein folding accessible to all. *Nat. Methods* **2022**, *19*, 679–682.

(39) Anandakrishnan, R.; Aguilar, B.; Onufriev, A. H++ 3.0: Automating pK prediction and the preparation of biomolecular structures for atomistic molecular modeling and simulations. *Nucleic Acids Res.* **2012**, *40*, W537–41.

(40) Mariani, V.; Biasini, M.; Barbato, A.; Schwede, T. lDDT: a local superposition-free score for comparing protein structures and models using distance difference tests. *Bioinformatics* **2013**, *29*, 2722–2728.

(41) Perkins, E. G. In *Practical Handbook of Soybean Processing and Utilization*; Erickson, D. R., Ed.; AOCS Press, 1995; pp 9–28.

(42) Jorgensen, W. L.; Tirado-Rives, J. Potential energy functions for atomic-level simulations of water and organic and biomolecular systems. *Proc. Natl. Acad. Sci. U. S. A.* **2005**, *102*, 6665–6670.

(43) Dodda, L. S.; Vilseck, J. Z.; Tirado-Rives, J.; Jorgensen, W. L. 1.14*CM1A-LBCC: Localized Bond-Charge Corrected CM1A Charges for Condensed-Phase Simulations. *J. Phys. Chem. B* **2017**, *121*, 3864–3870.

(44) Dodda, L. S.; Cabeza de Vaca, I.; Tirado-Rives, J.; Jorgensen, W. L. LigParGen web server: an automatic OPLS-AA parameter generator for organic ligands. *Nucleic Acids Res.* **2017**, *45*, W331–W336.

(45) Mark, P.; Nilsson, L. Structure and Dynamics of the TIP3P, SPC, and SPC/E Water Models at 298 K. *J. Phys. Chem. A* **2001**, *105*, 9954–9960.

(46) Jorgensen, W. L.; Jenson, C. Temperature dependence of TIP3P, SPC, and TIP4P water from NPT Monte Carlo simulations: Seeking temperatures of maximum density. *J. Comput. Chem.* **1998**, *19*, 1179–1186.

(47) Ali, A. H.; Zou, X.; Lu, J.; Abed, S. M.; Yao, Y.; Tao, G.; Jin, Q.; Wang, X. Identification of phospholipids classes and molecular species in different types of egg yolk by using UPLC-Q-TOF-MS. *Food Chem.* **2017**, *221*, 58–66.

(48) Jämbeck, J. P. M.; Lyubartsev, A. P. An Extension and Further Validation of an All-Atomistic Force Field for Biological Membranes. *J. Chem. Theory Comput.* **2012**, *8*, 2938–2948.

(49) Ermilova, I.; Lyubartsev, A. P. Extension of the Slipids Force Field to Polyunsaturated Lipids. *J. Phys. Chem. B* **2016**, *120*, 12826–12842.

(50) Abraham, M. J.; Murtola, T.; Schulz, R.; Páll, S.; Smith, J. C.; Hess, B.; Lindahl, E. GROMACS: High performance molecular simulations through multi-level parallelism from laptops to supercomputers. *SoftwareX* **2015**, *1-2*, 19–25.

(51) Essmann, U.; Perera, L.; Berkowitz, M. L.; Darden, T.; Lee, H.; Pedersen, L. G. A smooth particle mesh Ewald method. *J. Chem. Phys.* **1995**, *103*, 8577–8593.

(52) Berendsen, H. J. C. In *Computer Simulation in Materials Science: Interatomic Potentials, Simulation Techniques and Applications*; Meyer, M., Pontikis, V., Eds.; Springer Netherlands: Dordrecht, 1991; pp 139–155.

(53) Parrinello, M.; Rahman, A. Polymorphic transitions in single crystals: A new molecular dynamics method. *J. Appl. Phys. (Melville, NY, U. S.)* **1981**, *52*, 7182–7190.

(54) Bussi, G.; Donadio, D.; Parrinello, M. Canonical sampling through velocity rescaling. *J. Chem. Phys.* **2007**, *126*, 014101.

(55) Jorgensen, W. L.; Madura, J. D.; Swenson, C. J. Optimized intermolecular potential functions for liquid hydrocarbons. *J. Am. Chem. Soc.* **1984**, *106*, 6638–6646.

(56) Hess, B.; Bekker, H.; Berendsen, H. J. C.; Fraaije, J. G. E. M. LINCS: A linear constraint solver for molecular simulations. *J. Comput. Chem.* **1997**, *18*, 1463–1472.

(57) Jorgensen, W. L.; Chandrasekhar, J.; Madura, J. D.; Impey, R. W.; Klein, M. L. Comparison of simple potential functions for simulating liquid water. *J. Chem. Phys.* **1983**, *79*, 926–935.

(58) Miyamoto, S.; Kollman, P. A. Settle: An analytical version of the SHAKE and RATTLE algorithm for rigid water models. *J. Comput. Chem.* **1992**, *13*, 952–962.

(59) Humphrey, W.; Dalke, A.; Schulten, K. VMD: visual molecular dynamics. *J. Mol. Graphics* **1996**, *14*, 33–38.

(60) Bonomi, M.; Branduardi, D.; Bussi, G.; Camilloni, C.; Provasi, D.; Raiteri, P.; Donadio, D.; Marinelli, F.; Pietrucci, F.; Broglia, R. A.; Parrinello, M. PLUMED: A portable plugin for free-energy calculations with molecular dynamics. *Comput. Phys. Commun.* **2009**, *180*, 1961–1972.

(61) Tribello, G. A.; Bonomi, M.; Branduardi, D.; Camilloni, C.; Bussi, G. PLUMED 2: New feathers for an old bird. *Comput. Phys. Commun.* **2014**, *185*, 604–613.

(62) Tiwary, P.; Parrinello, M. A time-independent free energy estimator for metadynamics. *J. Phys. Chem. B* **2015**, *119*, 736–742.

(63) Fainerman, V. B.; Lucassen-Reynders, E. H.; Miller, R. Description of the adsorption behaviour of proteins at water/fluid interfaces in the framework of a two-dimensional solution model. *Adv. Colloid Interface Sci.* **2003**, *106*, 237–259.

(64) Fainerman, V. B.; Miller, R.; Ferri, J. K.; Watzke, H.; Leser, M. E.; Michel, M. Reversibility and irreversibility of adsorption of surfactants and proteins at liquid interfaces. *Adv. Colloid Interface Sci.* **2006**, *123-126*, 163–171.

(65) Graham, D. E.; Phillips, M. C. Proteins at liquid interfaces: II. Adsorption isotherms. *J. Colloid Interface Sci.* **1979**, *70*, 415–426.

(66) Zhou, X.; Zhou, X. THE UNIT PROBLEM IN THE THERMODYNAMIC CALCULATION OF ADSORPTION USING THE LANGMUIR EQUATION. *Chem. Eng. Commun.* **2014**, *201*, 1459–1467.

(67) Maldonado-Valderrama, J.; Fainerman, V. B.; Aksenenko, E.; Jose Gálvez-Ruiz, M.; Cabrerizo-Vílchez, M. A.; Miller, R. Dynamics of protein adsorption at the oil–water interface: comparison with a theoretical model. *Colloids Surf., A* **2005**, *261*, 85–92.

(68) Hayashi, A.; Ato, Y.; Yamamoto, A.; Yoshida, H.; Yamanaka, S.; Kawakami, T.; Okumura, M. Gibbs Energy of Hydrogen Adsorption on Pt Surface by Machine Learning Potential and Metadynamics. *Chem. Lett.* **2021**, *50*, 1329–1332.

(69) Norde, W.; Haynes, C. A. In *Interfacial phenomena and bioproducts*; Brash, J. L., Wojciechowski, P. W., Eds.; Marcel Dekker: New York, USA, 1996; pp 123–144.

(70) Ferrari, M.; Handgraaf, J.-W.; Boccardo, G.; Buffo, A.; Vanni, M.; Marchisio, D. L. Dataset for “Molecular modeling of the interface of an egg yolk protein-based emulsion". Zenodo, 2021; Dataset.

TOC Graphic

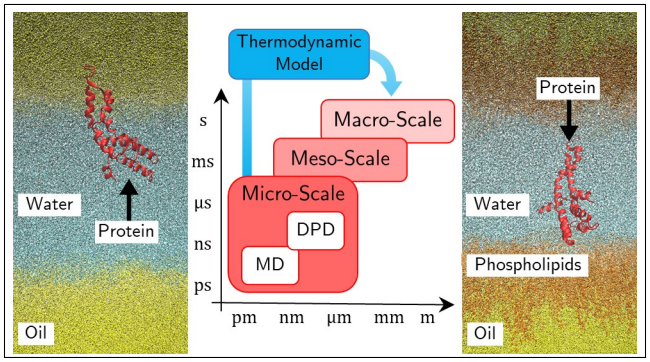
Water
Protein
Oil
Thermodynamic Model
Macro-Scale
Meso-Scale
Micro-Scale
DPD
MD
s
ms
µs
ns
ps
pm
nm
µm
mm
m
Protein
Water
Phospholipids
Oil